Aleksandar Bodić, Đorđe Ivković, Vladimir Dunić, Dušan Arsić, Miroslav Živković*

PHASE-FIELD DAMAGE MODELLING OF HIGH-STRENGTH STEEL FAILURE: NUMERICAL AND EXPERIMENTAL VALIDATION

MODELIRANJE LOMA ČELIKA POVIŠENE ČVRSTOĆE PRIMENOM METODE FAZNOG POLJA: NUMERIČKA I EKSPERIMENTALNA VALIDACIJA

Originalni naučni rad / Original scientific paper
Rad primljen / Paper received: 23.02.2026
https://doi.org/10.69644/ivk-2026-siA-0097
Adresa autora / Author's address:
University of Kragujevac, Faculty of Engineering, Kragujevac, Serbia A. Bodić https://orcid.org/0000-0002-1713-6540 ;
Đ. Ivković https://orcid.org/0000-0002-5747-7876 ,
*email: djordje.ivkovic@fink.rs ;
V. Dunić https://orcid.org/0000-0003-1648-1745 ;
D. Arsić https://orcid.org/0000-0003-0326-0898 ;
M. Živković https://orcid.org/0000-0002-0752-6289

Keywords
- finite element method
- phase-field damage model
- S1100QL steel
- PAK-DAM software

Abstract

Phase-field damage modelling (PFDM) has emerged as an effective framework for simulating a material degradation and failure processes due to its ability to predict the evolution of damage. In this study, a 2D axisymmetric PFDM formulation is verified in PAK-DAM FEM software through comparison with 3D solid model for benchmark example from the literature. After that, 2D axisymmetric FE model is used for a comparison with experimental tensile tests of high-strength S1100QL steel. The finite element model is developed using 2D axisymmetric elements, incorporating large-strain von Mises plasticity with a logarithmic strain constitutive model. The FE mesh consists of 970 elements and 1078 nodes, with boundary and loading conditions defined to replicate the experimental setup. A comparison of stress-strain response obtained from numerical simulations and experimental measurements shows good agreement, confirming the capability of the proposed PFDM approach to accurately reproduce the tensile behaviour of metallic materials such as S1100QL steel.

Ključne reči
- metoda konačnih elemenata
- model faznog polja sa oštećenjem
- S1100QL čelik
- PAK-DAM softver

Izvod

Modeliranje oštećenja metodom faznog polja (PFDM) predstavlja efikasan pristup za simulaciju procesa degradacije i loma materijala zahvaljujući sposobnosti da predvidi evoluciju oštećenja. U ovom radu, 2D osnosimetrična formulacija PFDM je verifikovana u MKE softveru PAK-DAM, poređenjem sa 3D modelom za referentni (benchmark) primer iz literature. Zatim je korišćen 2D osnosimetrični model konačnih elemenata za poređenje sa eksperimentalnim ispitivanjima zatezanjem čelika povišene čvrstoće S1100QL. Numerički model razvijen je korišćenjem 2D osnosimetričnih konačnih elemenata i primenom Von Misesovog konstitutivnog modela za velike deformacije, zasnovanog na logaritamskoj meri deformacije. Mreža konačnih elemenata sastoji se od 970 elemenata i 1078 čvorova, pri čemu su granični uslovi i opterećenja definisani tako da odgovaraju eksperimentu. Poređenje naponsko-deformacionog odziva iz numeričkih simulacija i eksperimentalnih merenja pokazuje dobro slaganje, čime se potvrđuje da predloženi PFDM pristup dovoljno tačno reprodukuje zatezno ponašanje čelika S1100QL.

INTRODUCTION

Steel structures are widely used in engineering applications due to their high load-carrying capacity and reliability and are typically designed to meet strict structural safety requirements /1, 2/. During service, however, such structures may be subjected to various loading conditions and environmental influences, including static and dynamic loading, cyclic loading, and material degradation, which can lead to excessive deformation, damage initiation, and structural failure /3, 4/. As a result, accurate characterisation and predictive modelling of fracture behaviour in metallic materials are essential for both the design of new structures and the integrity assessment of existing ones, /5/.

Modelling fracture in steel structures remains a challenging task. Classical fracture mechanics approaches based on Griffith's theory /6/ relate crack growth to the balance between elastic strain energy and surface energy and have proven effective for brittle materials. However, their application to ductile materials is limited, as crack initiation and propagation are strongly influenced by plastic deformation and energy dissipation mechanisms. Moreover, traditional approaches typically require a pre-existing crack and a predefined crack path, which restricts their applicability in complex structural analyses, /7, 8/.

To overcome these limitations, phase-field damage modelling (PFDM) has emerged as a robust and versatile framework for fracture simulation. By introducing a continuous damage variable governed by variational principles, PFDM enables a diffuse representation of cracks and allows for the natural modelling of crack initiation and propagation without explicit crack tracking. Because of this, PFDM has been increasingly integrated into finite element formulations and successfully applied to a wide range of fracture problems in metallic materials, /9-11/.

The phase-field damage models (PFDMs) were initially developed in the late 1990s and early 2000s as variational regularisations of Griffith's fracture theory, /12/. In particu-

lar, the contributions by Bourdin et al. /13/ introduced the use of a phase-field variable to provide a diffuse representation of cracks through the minimisation of the total energy functional of the system, thereby allowing the natural description of crack initiation and subsequent propagation. This variational framework was later refined and extended by numerous researchers /14-18/, leading to improved numerical robustness and broader applicability. Subsequent developments of PFDM have focused on its coupling with additional physical models, enabling the simulation of complex material behaviour such as elastoplasticity /19/, viscoelasticity /20/, anisotropy /21/, and thermomechanical effects /22/.

This paper is focused on the verification and validation of the 2D axisymmetric PFDM formulation within the in-house software PAK-DAM v25, /23/. This formulation was initially verified numerically by comparison with a 3D model of a benchmark example /24/ and then validated by comparison with experimental data of tensile tests of steel S1100QL.

In the second section, the critical-total strain-based formulation of PFDM is given. The third section presents the verification of the 2D axisymmetric PFDM formulation on 3D model of the benchmark example. In the fourth section, a description of experimental tensile tests of S1100QL steel is given. In the fifth section, a comparison of numerical simulation results with experimental data is given and conclusions are drawn at the end of the paper.

CRITICAL-TOTAL STRAIN BASED PHASE-FIELD DAMAGE MODEL

Griffith's fracture theory has served as a fundamental basis for the development of modern damage and fracture mechanics for more than a century, /6/. In this framework, the fracture criterion is formulated through the balance between the surface energy associated with crack formation and the elastic energy stored in the material. While this theory provides a reliable description of crack initiation from pre-existing flaws, it does not account for crack nucleation nor for subsequent crack propagation. To overcome these limitations, Francfort and Marigo /8/ introduced a variational formulation of fracture based on the minimisation of the total energy functional of the system. This approach was later regularised by means of a phase-field formulation, enabling a diffuse representation of cracks instead of a sharp discontinuity.

A commonly studied benchmark problem in the literature /25/ is an infinitely long bar with a constant cross-section containing a crack at its mid-length (Fig. 1). The material damage state, within this phase-field framework, is described by a scalar damage variable d which represents a quantitative measure of micro-cracks. In the sharp crack description in Eq.(1), the damage variable exhibits a localised discontinuity at the crack location. In contrast, for the diffuse crack topology adopted in phase-field damage models in Eq.(2), the damage is smoothly distributed along the axial coordinate.

$$d(x)=\begin{cases}1 & \text{if} \quad x=0\\ 0 & \text{if} \quad x\neq 0\end{cases}. \tag{1}$$

It can be given as an exponential function of the distance from the crack centre in following form:

$$d(x)=e^{-\frac{|x|}{l_c}}, \tag{2}$$

where: l_c represents the characteristic length parameter that governs the width of the damage localisation zone and controls the regularisation of the crack. When $l_c \to 0$, the diffuse formulation converges to the sharp crack representation in Eq.(1).

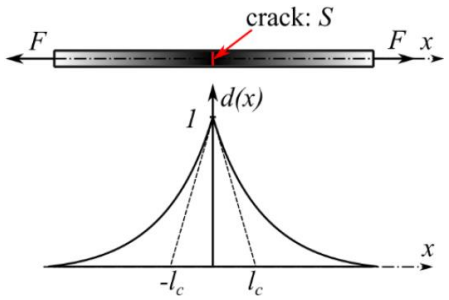

Figure 1. A bar loaded by forces F on both sides with a crack surface S in the middle: damage phase field for diffusive crack topology /5/.

This damage profile is the solution of the Euler-Lagrange equation associated with the regularised crack functional /7/:

$$d-l_c^2\nabla^2 d=0, \tag{3}$$

which follows from the minimisation of the crack surface functional.

For multi-dimensional problems, the regularised crack surface is defined as a volume integral, /5/:

$$\Gamma_l(d)=\int_V \gamma(d,\nabla d)\mathrm{d}V, \tag{4}$$

where the crack surface density function per unit volume is given by /5/:

$$\gamma(d,\nabla d)=\frac{d^2}{2l_c}+\frac{l_c}{2}\left|\nabla d\right|^2. \tag{5}$$

The total internal energy density of a damaged ductile solid is defined as the sum of elastic, plastic and fracture contributions, /25/:

$$\psi=\psi^E(\boldsymbol{\varepsilon}_E,d)+\psi^P(\bar{\varepsilon}_p,d)+\psi^S(d,\nabla d), \tag{6}$$

where the elastic energy density is degraded by a damage function $g(d)$:

$$\psi^E(\boldsymbol{\varepsilon}_E,d)=g(d)\frac{1}{2}\boldsymbol{\varepsilon}_E:\mathbf{C}_0:\boldsymbol{\varepsilon}_E, \qquad g(d)=(1-d)^2. \tag{7}$$

Accordingly, the Cauchy stress tensor in the damaged material reads /25/:

$$\boldsymbol{\sigma}=g(d)\mathbf{C}_0:\boldsymbol{\varepsilon}_E, \tag{8}$$

where: $\mathbf{C}_0$ represents fourth-order elastic constitutive matrix.

The fracture contribution to the energy is defined in terms of the critical fracture energy release rate G_c /7/:

$$\psi^S(d,\nabla d)=G_c\left(\frac{d^2}{2l_c}+\frac{l_c}{2}\left|\nabla d^2\right|\right). \tag{9}$$

The total internal potential energy functional of the system is then obtained by volume integration, /7/

$$\Psi=\int_V \psi \mathrm{d}V. \tag{1}$$

From the stationarity condition of the total potential energy with respect to the damage field, the governing phase-field evolution equation is obtained as, /25/:

$$G_c\left(d-l_c^2\nabla^2 d\right)+g'(d)\psi^E=0, \tag{11}$$

which couples damage evolution with the elastic energy density and governs crack initiation and propagation within the PFDM framework. More details about the theory background critical-total strain based PFDM can be found in the previous papers of the authors /7, 26-28/.

VERIFICATION OF 2D AXISYMMETRIC PFDM FORMULATION

The critical-total strain based PFDM implementation /7, 27/ in the PAK-DAM v25 /23/ software is verified for both 3D solid and 2D axisymmetric finite elements /28/ and tested on the classical circular bar necking problem from the literature /24/. Details about the implementation of the PFDM into the 2D axisymmetric finite element into the PAK-DAM FEM software are previously given in Dunić et al. /28/.

The modelled specimen has a bottom radius of 6.35 mm, a top radius 1 % larger (6.4135 mm), and a length of 26.67 mm; an imperfection is introduced at the smaller radius to initiate necking. Due to specimen symmetry, an eighth of the specimen is modelled with 648 3D hexahedral finite elements (3388 nodes), applying symmetry and displacement boundary conditions at the nodes on the bottom and the top surface of specimen, respectively. This model is about ten times larger and impractical to refine further. For 2D axisymmetric model a quarter of specimen cross-section is modelled with 96 elements (345 nodes), so that the element size corresponds to the 3D example. Boundary conditions for 2D axisymmetric model are set as follows: symmetry at the bottom and prescribed displacements on the opposite side, coupled through equations along the axis. The boundary conditions and loads for both 2D and 3D models are shown in Fig. 2.

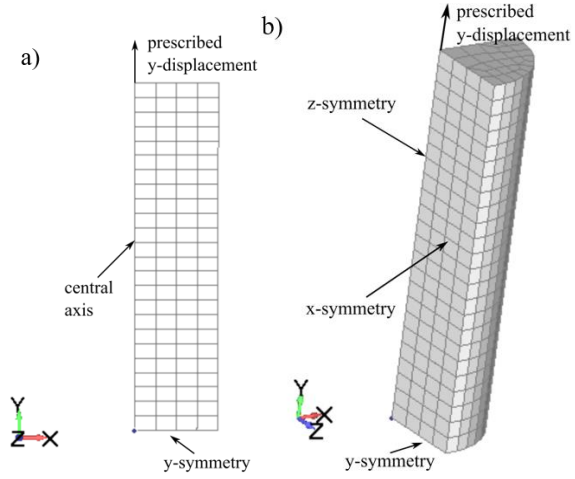

Figure 1. Boundary and loading conditions: a) 2D axisymmetric FE model; b) 3D solid FE model /28/.

It should be noted that the finite element mesh on both models is deliberately modelled coarse. The idea behind these initial calculations is to verify the 2D axisymmetric model by comparing it with the 3D results for a benchmark example from literature /24/. After initial verification simulations, this PFDM 2D axisymmetric formulation will be used for experimental testing.

A large strain von Mises plasticity constitutive model with logarithmic strain measure is used to capture the material response during deformation. Both models are solved using the Full Newton iterative method with line search, converging in 40 steps with 0.2 mm increment up to total displacement of 8 mm. Results are given in form of damage and equivalent plastic strain fields and damage field evolution for both 2D axisymmetric and 3D solid FE model.

The damage field in the last (40th) time step for 2D axisymmetric and 3D model is given in Fig. 3.

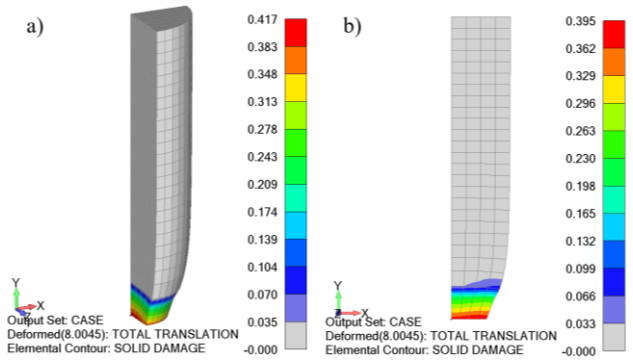

Figure 3. Damage field in the last (40th) time step for: a) 3D solid; and b) 2D axisymmetric FE model, /28/.

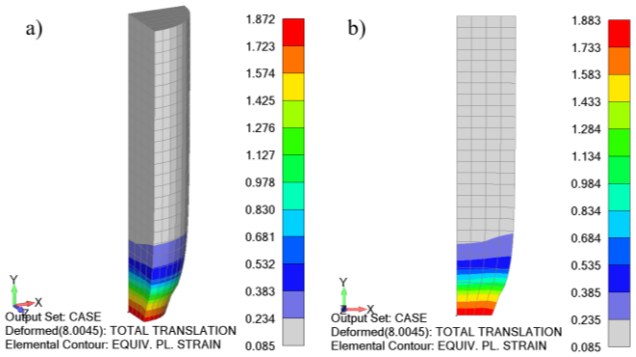

Figure 4. Equivalent plastic strain field in the last (40th) time step for: a) 3D solid; and b) 2D axisymmetric FE model, /28/.

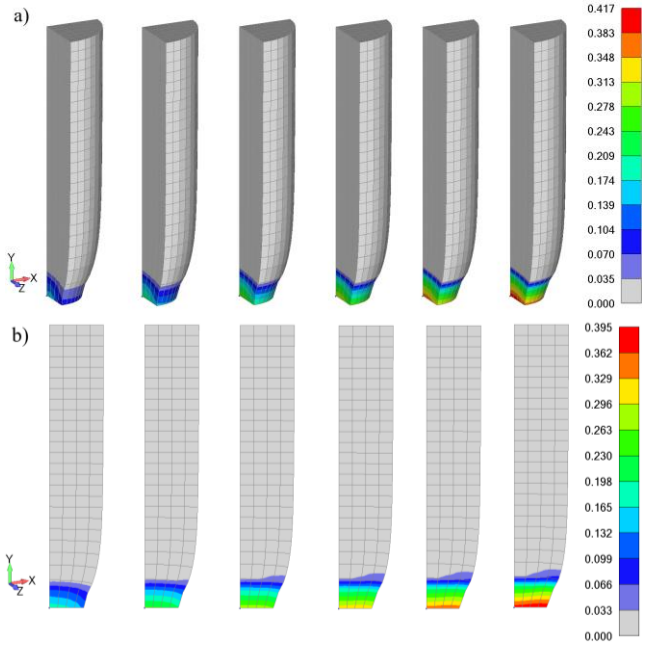

Figure 5. Damage field evolution in the last six time steps of the simulation (35th-40th, from left to right) for: a) 3D FE model; and b) 2D axisymmetric FE model, /28/.

The equivalent plastic strain field in the last (40th) time step for 2D axisymmetric and 3D model is given in Fig. 4.

Damage field evolution in the last six time steps (35-40th) for both 2D axisymmetric and 3D model is given in Fig. 5.

The comparison of the force vs. displacement diagram at the upper side of the model for 3D solid and 2D axisymmetric model is given in Fig. 6.

Results shown in Figs. 3-6 show very good agreement between 2D axisymmetric and 3D solid FE model for the benchmark example. It is important to point out that the calculation using the 2D axisymmetric FE model took significantly less time than using the 3D solid FE model (the calculation took 10 times less time). In this way, by using the 2D axisymmetric PFDM formulation in the in-house software package PAK-DAM v25, cylindrical test specimens that are standard for tensile testing of most metallic ductile materials can be numerically simulated much faster with the same accuracy.

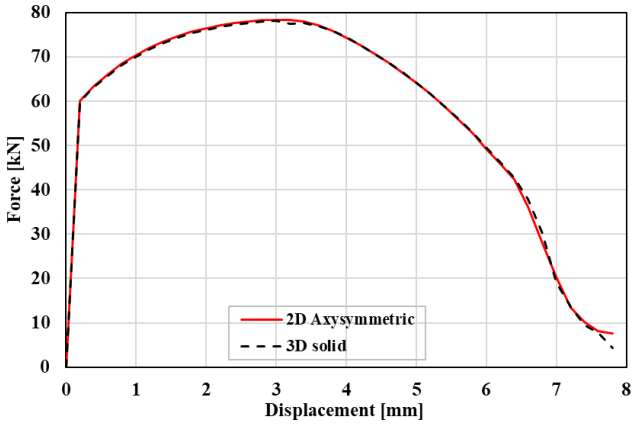

Figure 6. Force-displacement response for 3D solid FE model and 2D axisymmetric FE model.

EXPERIMENTAL TESTING OF S1100QL STEEL

In order to validate the proposed PFDM, experimental tensile tests are performed on specimens made of S1100QL ultra-high-strength structural steel. The experimental procedure and methodology following the investigation are reported in /29/. Similar methodology is used in earlier research of different steel groups, /30, 31/.

Cylindrical tensile specimens (Fig. 7) are machined from SSAB STRENX 1100 E/F plates using CNC turning operations in order to achieve high dimensional accuracy and uniform surface quality in the gauge section. The selected geometry corresponds to standard axisymmetric tensile specimens commonly used for high-strength steels and is particularly suitable for subsequent numerical simulation using a 2D axisymmetric finite element formulation. Special care is taken to avoid machining-induced surface defects that could influence crack initiation.

Figure 7. Cylindrical tensile specimens.

Tensile testing is conducted on a universal testing machine ZWICK ROELL Z/100 (ZWICKROELL GmbH, Ulm, Germany), Fig. 8. The tests are carried out under displacement control with a constant crosshead speed of 10 mm/min. During testing, the applied load and axial displacement are continuously recorded. For each testing condition, two specimens are tested to ensure the repeatability of results.

Figure 8. ZWICK ROELL Z/100 testing machine.

Engineering stress-strain curves are constructed from the recorded force-displacement data. The 0.2 % proof stress ($R_{p0.2}$), ultimate tensile strength (R_m), and total elongation (A) are determined according to standard tensile testing procedures. The obtained results at room temperature confirm the ultra-high-strength character of the material. The measured yield strength exceeds 1100 MPa, while the ultimate tensile strength ranges approximately between 1390 MPa and 1400 MPa, which is in good agreement with the manufacturer's declared properties and previously reported experimental data /29/. The total elongation is lower than nominal catalogue values, which is characteristic for quenched and tempered martensitic steels of this strength level and reflects limited uniform plastic deformation. The stress-strain response exhibits high initial stiffness, followed by a relatively short region of uniform plastic deformation and pronounced strain localisation prior to fracture. After reaching the maximal load, necking develops rapidly, leading to ductile failure. Such behaviour is typical for ultra-high-strength martensitic steels and is particularly relevant for phase-field damage modelling, since the onset of damage is closely related to strain localisation mechanisms.

For numerical simulations, the true stress-strain relationship is reconstructed from the experimentally obtained engineering curve. Up to the onset of necking, the conversion from engineering to true stress and strain is performed using logarithmic relations. Beyond uniform elongation, the procedure proposed in /29/ is applied in order to account for the reduction of the cross-sectional area during plastic deformation and to determine actual material response. The resulting true stress-strain curve is used for calibration of the isotropic hardening elastoplastic constitutive model in PAK-DAM v25 and serves as input for subsequent phase-field damage modelling.

VERIFICATION OF 2D AXISYMMETRIC PFDM FORMULATION ON 3D FE MODEL

Experimental tests shown in the previous chapter are simulated using PAK-DAM v25 software. Numerical simulations are conducted using 2D axisymmetric finite elements. Dimensions of the created FE model correspond to real specimen dimensions used in experimental tests. The axisymmetric *r-z* cross-section of half of the cylindrical specimen is modelled using 970 2D axisymmetric finite elements and 1078 nodes. Boundary conditions are set to correspond real testing conditions: symmetry is set at the nodes on the bottom edge of the model and prescribed displacements are defined at nodes on the upper edge of the specimen, coupled through equations along the axis. 2D axisymmetric FE model of specimen with boundary conditions is given in Fig. 9.

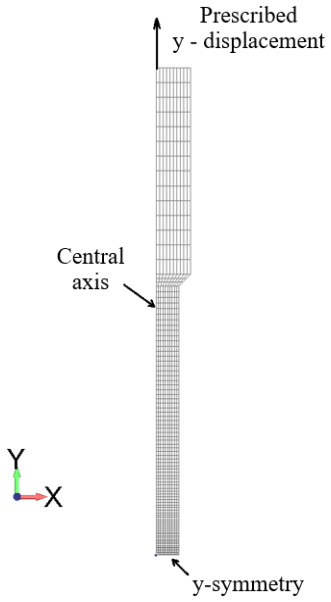

Figure 9. 2D axisymmetric FE specimen model with boundary conditions.

An isotropic hardening plasticity model is used for defining plastic behaviour of specimen, coupled with PFDM. Material constants are determined by fitting constitutive model parameters and given in Table 1.

The model is solved using Full Newton iterative method with line search in 80 steps with 0.125 mm increments up to a total displacement of 6.625 mm. The damage field in the last converged (53rd) time step is given in Fig. 10.

Table 1. Material parameters for numerical simulations.

Material parameter	Value	Unit
Young's modulus - E	210	GPa
Poisson's ration - ν	0.3	-
Yield stress - σ_{yv}	1.09	GPa
Saturation hardening stress - $\sigma_{y0,\infty}$	1.467	GPa
Hardening exponent - n	50.4	-
Hardening modulus - H	0.8	GPa
Critical effective plastic strain - e_{cr}	1.05	-
Characteristic length - l	0.5	mm

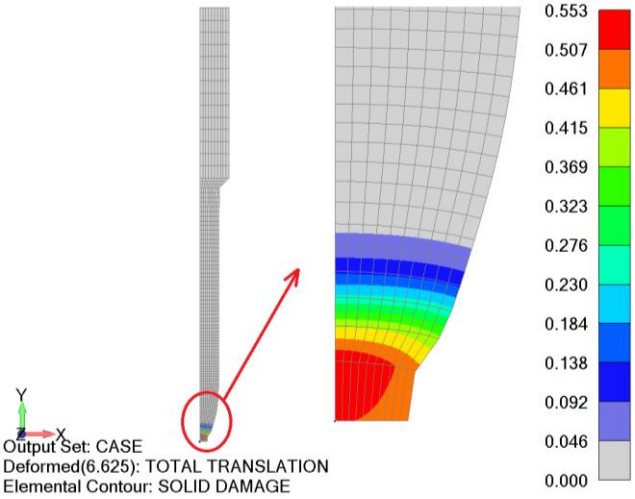

Figure 10. Damage field in last converged (53rd) time step.

The equivalent plastic strain field in the last converged (53rd) time step for is given in Fig. 11.

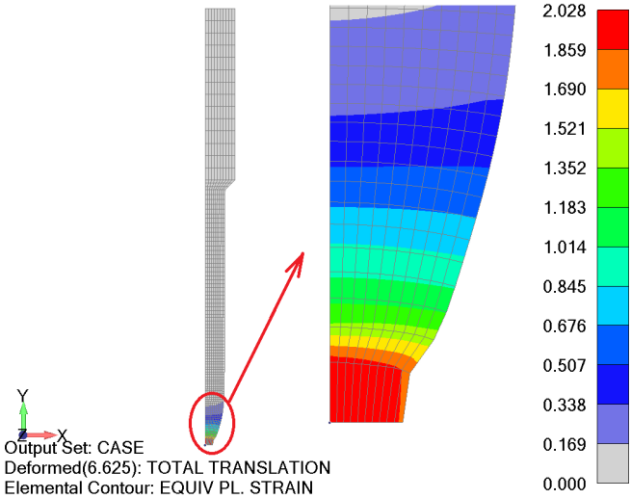

Figure 11. Equivalent plastic strain field in last converged (53rd) time step.

Damage field evolution in the last four time-steps (50th-53rd) of the simulation is given in Fig. 12.

Comparison of stress-strain curve /32/ for numerical simulation and experiment is given in Fig. 13.

The results given in Figs. 10-13 show good agreement between experimental and numerical results. This confirms that numerical simulations based on the phase-field damage model (PFDM) are capable of accurately reproducing the mechanical response of cylindrical specimen subjected to tensile loading, in close correspondence with the experi-

mental results. Furthermore, the 2D axisymmetric PFDM formulation for the cylindrical specimen significantly reduces computational time and resource requirements, thereby contributing to additional savings in engineering effort and experimental costs.

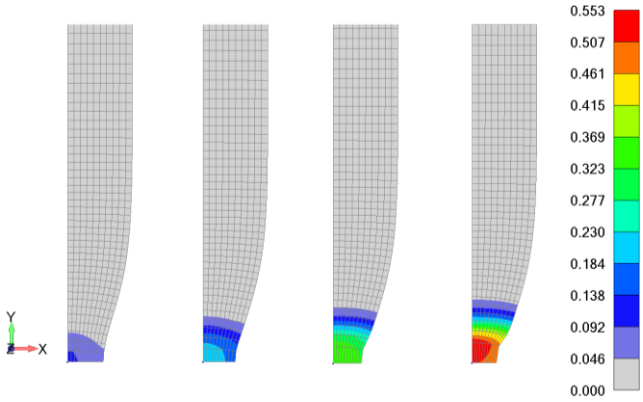

Figure 12. Damage field evolution in the last four time-steps of the simulation (50th-53rd, from left to right).

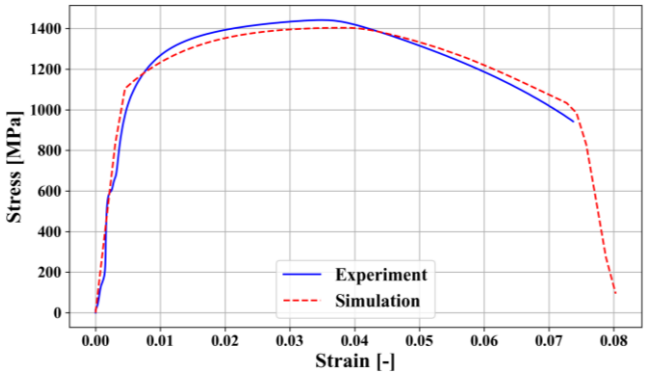

Figure 13. Comparison of stress-strain curve for experiment and simulation.

CONCLUSIONS

In this study, the 2D axisymmetric PFDM framework in the PAK-DAM v25 software is firstly verified through comparison with a 3D finite element model for a benchmark problem, demonstrating excellent agreement in terms of damage evolution and global mechanical response. Subsequently, the 2D axisymmetric PFDM model is validated on the experimental tensile test results obtained from cylindrical specimens. The experimental tensile tests are performed on S1100 QL high strength steel specimens. Numerical simulations accurately reproduce the experimentally observed stress-strain response and damage localisation, confirming the capability of the proposed approach to capture the tensile behaviour and failure characteristics of the material. By applying this 2D axisymmetric PFDM finite element, a significant reduction in computational time and resource requirements is achieved compared to the full 3D model. The results indicate that the 2D axisymmetric PFDM formulation in PAK-DAM FEM software represents an efficient and reliable tool for the numerical analysis of ductile fracture in axisymmetric structural components, offering favourable balance between accuracy and computational efficiency.

ACKNOWLEDGEMENT

This research is partly supported by the Science Fund of the Republic of Serbia, GRANT No 7475, Prediction of damage evolution in engineering structures - PROMINENT, and by the Ministry of Science, Technological Development and Innovation, Republic of Serbia, Agreement No. 451-03-34/2026-03/200107.

The research presented in the paper is in line with Sustainable Development Goals 9: Industry, Innovation, and Infrastructure, and 12: Responsible Consumption and Production.

REFERENCES

1. Anderson, T.L., Fracture Mechanics: Fundamentals and Applications, 4th Ed., CRC Press, 2017. doi: 10.1201/9781315370293
2. Besson, J., Cailletaud, G., Chaboche, J.-L., et al. (2010), Introduction, In: Non-Linear Mechanics of Materials. Solid Mechanics and Its Applications, 167: 1-6. doi: 10.1007/978-90-481-3356-7_1
3. Lemaitre, J., Desmorat, R., Engineering Damage Mechanics: Ductile, Creep, Fatigue and Brittle Failures, Springer Berlin, Heidelberg, 2005. doi: 10.1007/b138882
4. Gross, D., Seelig, T., Fracture Mechanics: With an Introduction to Micromechanics, 3rd Ed., Springer Cham, 2018. doi: 10.1007/978-3-319-71090-7
5. Živković, J., Dunić, V., Milovanović, V., et al. (2021), *A modified phase-field damage model for metal plasticity at finite strains: Numerical development and experimental validation*, Metals, 11(1): 47. doi: 10.3390/met11010047
6. Griffith, A.A. (1921), *VI. The phenomena of rupture and flow in solids*, Phil. Trans. R. Society A, 221(582-593): 163-198. doi: 10.1098/rsta.1921.0006
7. Dunić, V., Gubeljak, N., Živković, M., et al. (2024), *Experimental characterization and phase-field damage modeling of ductile fracture in AISI 316L*, Metals, 14(7): 787. doi: 10.3390/met14070787
8. Francfort, G.A., Marigo, J.-J. (1998), *Revisiting brittle fracture as an energy minimization problem*, J Mech. Phys. Solids, 46 (8): 1319-1342. doi: 10.1016/S0022-5096(98)00034-9
9. Ambati, M., Gerasimov, T., De Lorenzis, L. (2015), *Phase-field modeling of ductile fracture*, Comput. Mech. 55(5): 1017-1040. doi: 10.1007/s00466-015-1151-4
10. Ambati, M., Gerasimov, T., De Lorenzis, L. (2015), *A review on phase-field models of brittle fracture and a new fast hybrid formulation*, Comput. Mech. 55(2): 383-405. doi: 10.1007/s00466-014-1109-y
11. Miehe, C., Hofacker, M., Welschinger, F. (2010), *A phase field model for rate-independent crack propagation: Robust algorithmic implementation based on operator splits*, Comput. Meth. Appl. Mech. Eng. 199(45-48): 2765-2778. doi: 10.1016/j.cma.2010.04.011
12. Bourdin, B., Francfort, G.A., Marigo, J.-J. (2008), *The variational approach to fracture*, J Elasticity, 91(1-3): 5-148. doi: 10.1007/s10659-007-9107-3
13. Bourdin, B., Francfort, G.A., Marigo, J.-J. (2000), *Numerical experiments in revisited brittle fracture*, J Mech. Phys. Solids, 48(4): 797-826. doi: 10.1016/S0022-5096(99)00028-9
14. Burke, S., Ortner, C., Süli, E. (2010), *An adaptive finite element approximation of a variational model of brittle fracture*, SIAM J Numer. Anal. 48(3): 980-1012. doi: 10.1137/080741033
15. Maso, G.D., Toader, R. (2001), *A model for the quasi-static growth of a brittle fracture: existence and approximation results*, arXiv. doi: 10.48550/ARXIV.MATH/0101089

16. Amor, H., Marigo, J.-J., Maurini, C. (2009), *Regularized formulation of the variational brittle fracture with unilateral contact: Numerical experiments*, J Mech. Phys. Solids, 57(8): 1209-1229. doi: 10.1016/j.jmps.2009.04.011
17. Miehe, C., Aldakheel, F., Raina, A. (2016), *Phase field modeling of ductile fracture at finite strains: A variational gradient-extended plasticity-damage theory*, Int. J Plasticity, 84: 1-32. doi: 10.1016/j.ijplas.2016.04.011
18. Ambati, M., Kruse, R., De Lorenzis, L. (2016), *A phase-field model for ductile fracture at finite strains and its experimental verification*, Comput. Mech. 57(1): 149-167. doi: 10.1007/s00466-015-1225-3
19. Li, P., Wu, Y., Yvonnet, J., et al. (2024), *Phase field modeling of dynamic fracture in elastoplastic composites with interfacial debonding*, Eng. Fract. Mech. 295: 109792. doi: 10.1016/j.engfracmech.2023.109792
20. Dammaß, F., Ambati, M., Kästner, M. (2021), *Phase-field modelling and simulation of fracture in viscoelastic materials*, Proc. Appl. Math. Mech. 21(1): e202100108. doi: 10.1002/pamm.202100108
21. Ruan, H., Peng, X.-L. (2025), *Phase-field modeling of anisotropic fracture of additively manufactured parts*, Eng. Fract. Mech. 323: 111160. doi: 10.1016/j.engfracmech.2025.111160
22. Tang, G., Guo, D., Zhong, W., et al. (2025), *Phase-field modeling of thermal fracturing mechanisms in reservoir rock under high-temperature conditions*, Appl. Sci. 15(15): 8693. doi: 10.3390/app15158693
23. Živković, M., Dunić, V., Rakić, D., et al. (2025), PAK-DAM Software for Damage and Fracture Simulation, University of Kragujevac, Faculty of Engineering, Kragujevac, Serbia, 2025.
24. Simo, J.C., Miehe, C. (1992), *Associative coupled thermoplasticity at finite strains: Formulation, numerical analysis and implementation*, Comput. Methods Appl. Mech. Eng. 98(1): 41-104. doi: 10.1016/0045-7825(92)90170-O
25. Živković, J., *Improvement, implementation and experimental verification of numerical modeling of damage and fracture of metals using phase-field modeling*, Ph.D. Thesis, University of Kragujevac, Kragujevac, Serbia, 2022.
26. Dunić, V., Matsui, R., Takeda, K., Živković, M. (2024), *Phase-field damage simulation of subloop loading in TiNi SMA*, Int. J Damage Mech. 33(8): 577-604. doi: 10.1177/10567895241245859
27. Dunić, V., Živković, M. (2026), *Critical total strain-based phase-field damage model for ductile fatigue*, In: Schäfer, M., et al., New Trends in Computational Engineering, ICCE 2024. Lecture Notes in Computational Science and Engineering, vol.150, Springer Cham. pp.73-83. doi: 10.1007/978-3-032-16253-3_5
28. Dunić, V., Bodić, A., Živković, M. (2025), *2D axisymmetric vs. 3D solid element phase-field damage modeling*, In: 41st Danubia-Adria Symp. Advances in Experimental Mechanics, University of Kragujevac, Faculty of Engineering, Kragujevac, Serbia, 2025, pp.139-142. doi: 10.46793/41DAS2025.139D
29. Ivković, D., Arsić, D., Radović, L., et al. (2025), *Investigation of tensile properties at room and elevated temperatures of S1100QL steel and its welded joints*, Coatings, 15(6): 696. doi: 10.3390/coatings15060696
30. Arsić, D., Djordjević, M., Živković, J., et al. (2016), *Experimental-numerical study of tensile strength of the high-strength steel S690QL at elevated temperatures*, Strength Mater. 48(5): 687-695. doi: 10.1007/s11223-016-9812-x
31. Arsić, D., Lazić, V., Sedmak, A., et al. (2020), *Effect of elevated temperatures on mechanical properties of ultra high strength hot work tool steel H11*, Trans. FAMENA, 44(2): 71-82. doi: 10.21278/TOF.44207
32. Milošević, N., Sedmak, A., Martić, I., Prokić-Cvetković, R. (2021), *Novel procedure to determine actual stress-strain curves*, Struct. Integr. Life, 21(1): 37-40.

© 2026 The Author. Structural Integrity and Life, Published by DIVK (The Society for Structural Integrity and Life 'Prof. Dr Stojan Sedmak') (http://divk.inovacionicentar.rs/ivk/home.html). This is an open access article distributed under the terms and conditions of the Creative Commons Attribution-NonCommercial-NoDerivatives 4.0 International License